

# Vetting quark-star models with gravitational waves in the hierarchical Bayesian framework

Ziming Wang,<sup>a,b</sup> Yong Gao,<sup>c</sup> Dicong Liang,<sup>d</sup> Junjie Zhao<sup>e</sup> and Lijing Shao<sup>b,f,1</sup>

<sup>a</sup>Department of Astronomy, School of Physics, Peking University, Beijing 100871, China

<sup>b</sup>Kavli Institute for Astronomy and Astrophysics, Peking University, Beijing 100871, China

<sup>c</sup>Max Planck Institute for Gravitational Physics (Albert Einstein Institute), Am Mühlenberg 1, D-14476 Potsdam-Golm, Germany

<sup>d</sup>Department of Mathematics and Physics, School of Biomedical Engineering, Southern Medical University, Guangzhou 510515, China

<sup>e</sup>Henan Academy of Sciences, Zhengzhou 450046, Henan, China

<sup>f</sup>National Astronomical Observatories, Chinese Academy of Sciences, Beijing 100012, China

E-mail: [zwang@pku.edu.cn](mailto:zwang@pku.edu.cn), [yong.gao@aei.mpg.de](mailto:yong.gao@aei.mpg.de), [dcliang@smu.edu.cn](mailto:dcliang@smu.edu.cn), [junjiezhao@hnas.ac.cn](mailto:junjiezhao@hnas.ac.cn), [lshao@pku.edu.cn](mailto:lshao@pku.edu.cn)

**Abstract.** The recent discovery of gravitational waves (GWs) has opened a new avenue for investigating the equation of state (EOS) of dense matter in compact stars, which is an outstanding problem in astronomy and nuclear physics. In the future, next-generation (XG) GW detectors will be constructed, deemed to provide a large number of high-precision observations. We investigate the potential of constraining the EOS of quark stars (QSs) with high-precision measurements of mass  $m$  and tidal deformability  $\Lambda$  from the XG GW observatories. We adopt the widely-used bag model for QSs, consisting of four microscopic parameters: the effective bag constant  $B_{\text{eff}}$ , the perturbative quantum chromodynamics correction parameter  $a_4$ , the strange quark mass  $m_s$ , and the pairing energy gap  $\Delta$ . With the help of hierarchical Bayesian inference, for the first time we are able to infer the EOS of QSs combining multiple GW observations. Using the top 25 loudest GW events in our simulation, we find that, the constraints on  $B_{\text{eff}}$  and  $\Delta$  are tightened by several times, while  $a_4$  and  $m_s$  are still poorly constrained. We also study a simplified 2-dimensional (2-d) EOS model which was recently proposed in literature. The 2-d model is found to exhibit significant parameter-estimation biases as more GW events are analyzed, while the predicted  $m$ - $\Lambda$  relation remains consistent with the full model.

---

<sup>1</sup>Corresponding author.

---

## Contents

<b>1</b>	<b>Introduction</b>	<b>1</b>
<b>2</b>	<b>QS Models and GW Signals</b>	<b>2</b>
2.1	EOS of Qs and Tidal Deformability	2
2.2	Population, Waveform and Detectors of GWs	4
<b>3</b>	<b>Hierarchical Inference of EOS Parameters</b>	<b>6</b>
3.1	Principles	6
3.2	Implementation	8
<b>4</b>	<b>Results and Discussions</b>	<b>9</b>
4.1	Inference of Parameters in the 4-d Model	9
4.2	Comparison between 2-d and 4-d Models	10
<b>5</b>	<b>Summary and Outlook</b>	<b>12</b>

---

## 1 Introduction

The state of dense matter in compact stars has been a long-standing problem in astronomy and nuclear physics, which originates from the complexity of nonperturbative quantum chromodynamics (QCD). Besides the commonly adopted neutron star (NS) models, self-bound quark stars (Qs) were also proposed as a candidate for compact stars. Qs are entirely occupied by strange quark matter (SQM), where the SQM forms the true ground state [1–6]. Qs are considered as an important candidate for pulsars, and the properties of SQM can be constrained by measurements of mass and/or radius in pulsar observations. To be consistent with current observation of high-mass pulsars, one has to take into account the effects from strong interaction, such as one-gluon exchange or color-superconductivity, to increase the maximum mass of Qs [7–12]. Using the theoretically calculated maximum mass, one can place constraints on the equation of state (EOS) of compact stars, which gives the relationship between the pressure and the energy density of the dense matter [13–18]. Besides the maximum mass, the radius inferred from electromagnetic observations can provide additional constraints on the EOS of Qs [17, 19].

Recently, the discovery of gravitational waves (GWs) [20] has opened a new window for studying the EOS of compact stars. When one compact star orbits around the other in a close orbit, it gets deformed due to the tidal force exerted by the companion’s gravitational field. Such tidal deformation affects the inspiral of the binary, thus it is manifested in the phase evolution of GWs [21–25]. Given the mass of a compact star, its tidal deformability, which is a measure of the star’s response to the external gravitational field, is determined by the EOS. Consequently, the information about the EOS can be inferred from GW signals [26–40]. Other properties of GW events, such as the oscillation frequencies of post-merger remnants and the electromagnetic counterparts, can also provide information on the EOS [41–49].

In the future, the next-generation (XG) GW detectors, such as the Cosmic Explorer (CE) [50, 51] and the Einstein Telescope (ET) [52–54] will be constructed. Due to their largely increased sensitivity and a lower cutoff frequency, many more compact binary coalescence

signals are expected to be detected, reaching  $10^5$ – $10^6$  events per year [55–58]. Previous studies have introduced the hierarchical Bayesian inference techniques to combine numerous GW events and draw information from populations of GW events [59–64]. In this case, as the EOS determines the relationship between the tidal deformability  $\Lambda$  and the mass  $m$  of compact stars, the EOS parameters can be regarded as hyper-parameters and incorporated into the framework of hierarchical Bayesian inference. There are many studies using this technique to investigate the prospects of exploring the EOS of NSs in the XG GW detector era, finding that the EOS will be tightly constrained with the help of high-precision observation and the accumulation of GW events [46, 65–73].

As for the QS model, current studies mostly have used the detected GW events so far, namely, GW170817, GW190425 and GW190814, to constrain the EOS parameters in the bag model of QSs [74–85]. However, there is still a lack of discussion for the potential of constraining the QS model when combining multiple GW events from future GW observatories. Recently, Zhang and Mann [77] proposed a unified QS EOS including the nonzero strange quark mass, perturbative (QCD) corrections and color superconductivity. It has four model parameters, and we will call it the 4-dimensional (4-d) model. In this model, by omitting the fourth and higher order terms of the strange quark mass in the chemical potential, the EOS model has an analytical form, and it reduces the number of free parameters from four to two. This approximation, which we call the 2-d model, is accurate enough for current observational constraints, but may lead to significant biases when it is applied to fit high-precision measurements from XG GW observations.

In this work, in the framework of hierarchical Bayesian inference, we investigate the potential of constraining the EOS of QSs with multiple GW events in the XG detectors, and compare the behaviors of the 4-d model and the approximated 2-d model in the EOS inference. We find that the parameter estimation (PE) biases of the 2-d model becomes significant as the number of GW events accumulates, while the predicted  $m$ - $\Lambda$  relation is still consistent with the 4-d model and the injected EOS. Therefore, we conclude that, in the EOS inference of QSs with the XG detector observations, the approximated but analytical 2-d model is a good choice for a rapid inference of the  $m$ - $\Lambda$  relation, while there is still a need for a full inference using the full (4-d) model to ensure a correct understanding of the microscope physics.

The rest of this paper is organized as follows. In section 2, we introduce the EOS model of QSs and the setting of our simulation. Section 3 describes the methodology of hierarchical Bayesian inference and the specifics to apply it to the EOS inference. In section 4, we present the inference results of the full and approximated QS models. We summarize and discuss our results in section 5.

## 2 QS Models and GW Signals

### 2.1 EOS of QSs and Tidal Deformability

SQM consists of nearly equal numbers of up (u), down (d), and strange (s) quarks, with a small fraction of electrons to maintain charge neutrality. Since directly solving the EOS for QSs is not feasible, various models have been proposed to describe SQM [80]. The most popular one is the MIT bag model with first-order corrections from the perturbative QCD, effects from finite strange quark mass, and possible existence of color superconductivity [4–6].

The thermodynamical potential density can be written as [5, 6, 15]

$$\Omega = \sum_{i=u, d, s, e^-} \Omega_i^0 + \frac{3(1-a_4)}{4\pi^2} \mu^4 + B_{\text{eff}} + \frac{3m_s^4 - 48\Delta^2 \mu^2}{16\pi^2}, \quad (2.1)$$

where  $\Omega_i^0$  represents the potential for type  $i$  particle described as non-interacting fermions,  $\mu = \sum_i \mu_i/3$  is the average chemical potential of the quark matter. We neglect the mass of u and d quarks, and denote the mass of s quark as  $m_s$ . The effective bag constant  $B_{\text{eff}}$  accounts for the contributions from the QCD vacuum. The parameter  $a_4$  is commonly taken to be  $2\alpha_s/\pi$  to one-loop order with  $\alpha_s$  being the strong coupling constant [86, 87]. Note that both  $B_{\text{eff}}$  and  $a_4$  are effective parameters characterizing non-perturbative effects of the strong interactions. The last term in Eq. (2.1) is added when the SQM is in a color-flavor locked state, with the pairing gap  $\Delta$  on the order of tens to a hundred MeV [88]. In short, in this model we use four parameters, namely,  $\{B_{\text{eff}}^{1/4}, a_4, m_s, \Delta\}$ , to parametrize the QS EOS.

Zhang and Mann [77] reformulated the thermodynamic potential density in Eq. (2.1) by neglecting the contributions from electrons and omitting terms of order  $\mathcal{O}(m_s^4)$  and higher, and obtained,

$$\Omega = -\frac{3}{4\pi^2} \mu^4 + \frac{3(1-a_4)}{4\pi^2} \mu^4 - \frac{3\Delta^2 - 3m_s^2/4}{\pi^2} \mu^2 + B_{\text{eff}}. \quad (2.2)$$

Using the newly defined parameter,

$$\beta = \frac{3\Delta^2 - 3m_s^2/4}{\sqrt{3a_4}}, \quad (2.3)$$

Zhang and Mann [77] reparametrized the EOS using only two parameters  $\{B_{\text{eff}}^{1/4}, \beta\}$ . This approximation is accurate enough to describe SQM in most parameter space, especially for a small value of  $m_s$ .

The pressure, energy density, and baryon number density can be obtained through the grand potential in Eqs. (2.1–2.2) [5]. By solving the Tolman-Oppenheimer-Volkoff (TOV) equation one can obtain the mass  $m$  and radius  $R$  of QSs. The tidal deformability parameter  $\lambda$  of QSs/NSs is defined as the ratio of the induced quadrupole deformation to the tidal field of the companion [89]. The parameter  $\lambda$  can be written as

$$\lambda = \frac{2}{3} k_2 R^5. \quad (2.4)$$

Here the dimensionless parameter  $k_2$  is the so-called Love number, which can be calculated from perturbation theory in the General Relativity [89]. The dimensionless tidal deformability is defined as  $\Lambda = \lambda/m^5$ . In figure 1, we present the  $m$ - $\Lambda$  relation using the parameters  $B_{\text{eff}}^{1/4} = 140$  MeV,  $a_4 = 0.8$ ,  $m_s = 100$  MeV, and  $\Delta = 50$  MeV. The corresponding parameter  $\beta$  for the 2-d model can be calculated from Eq. (2.3). In this case, the relative difference in the tidal deformability between the 2-d and 4-d models is approximately 5%.

The Bodmer-Witten conjecture [2, 3] indicates that the SQM is the ground state of strong interactions. Consequently, the energy per baryon of SQM,  $(E/A)_{\text{uds}}$ , must be lower than that of  $^{56}\text{Fe}$ , specifically  $(E/A)_{\text{uds}} \leq 930\text{MeV}$  [2, 3]. Additionally, by imposing  $(E/A)_{\text{ud}} \geq 934\text{MeV}$  for the two-flavor quark matter in its ground state, one ensures that atomic nuclei remain stable and do not dissolve into their constituent quarks [90]. Given the specific EOS of SQM, one obtains the mass-radius relation and the corresponding maximal mass of QSs,

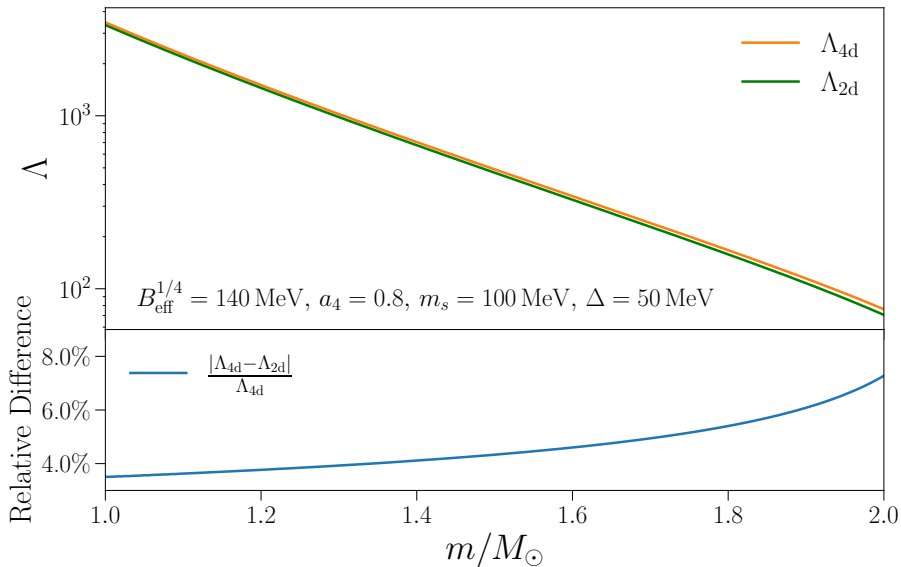


**Figure 1.** The upper panel shows the relation between the dimensionless tidal deformability  $\Lambda$  and the mass  $m$  for 2-d and 4-d models. In the 4-d model, parameters are  $B_{\text{eff}}^{1/4} = 140$  MeV,  $a_4 = 0.8$ ,  $m_s = 100$  MeV, and  $\Delta = 50$  MeV. The lower panel shows the relative difference in the tidal deformability between the 2-d and 4-d models.

$M_{\text{TOV}}$ . The mass measurements of massive pulsars provide a lower bound on the maximum mass of QSSs. Currently, the most massive pulsar observed to date is PSR J0740+6620, with  $m = 2.072_{-0.066}^{+0.067} M_{\odot}$  (68% confidence level) [91]. Only EOSs that support a maximum mass  $m_{\text{TOV}}$  exceeding this lower bound can satisfy the observation of PSR J0740+6620. Note that the illustrated case in figure 1 satisfies the above three constraints.

## 2.2 Population, Waveform and Detectors of GWs

This subsection describes how in the simulation we generate the GW signals, consisting of the population model and waveform template for GW sources, and the detector configuration for GW observations.

We adopt the mass population model of merging binaries given by Farrow *et al.* [92] for QSSs. The distribution of the primary mass  $m_1$  has two Gaussian components,

$$P(m_1) = \gamma_{\text{NS}} \mathcal{N}(\mu_1, \sigma_1) + (1 - \gamma_{\text{NS}}) \mathcal{N}(\mu_2, \sigma_2), \quad (2.5)$$

where  $\gamma_{\text{NS}} = 0.68$ ,  $\mu_1 = 1.34 M_{\odot}$ ,  $\sigma_1 = 0.02 M_{\odot}$ ,  $\mu_2 = 1.47 M_{\odot}$ , and  $\sigma_2 = 0.15 M_{\odot}$ . Sometimes we still use the notation “NS”, but it is clear from the context that we are considering QSSs. The secondary mass  $m_2$  is drawn from a uniform distribution,  $\mathcal{U}(1.14 M_{\odot}, 1.46 M_{\odot})$ . Considering formation and evolution models, neither of the binary components are likely to have high spins, so we neglect the spin effects of the QSSs, just like what Golomb and Talbot [69] did for NSs.

For the extrinsic parameters of GWs, we draw the merging binaries with isotropically distributed positions and orientations. Using the cosmological parameters provided by the Planck Collaboration [93], we generate 1000 GW events within 500 Mpc uniformly distributed in the comoving volume. This corresponds to several years’ observation for a uniform local merger rate  $R = 320_{-270}^{+490} \text{ Gpc}^{-3} \text{ yr}^{-1}$  from the current GW detectors [94]. It is found that

the major information about the EOS is obtained from the loudest several events in the population [65]. To reduce the calculation cost, we only select the 25 sources with the highest signal-to-noise ratio (SNR) for Bayesian analysis, leaving a more comprehensive study using the full population for future work. All GW signals are injected with an arbitrary merger time  $t_c = 0$ .

For the tidal deformability parameter, we adopt the 4-d QS model to inject the dimensionless tidal deformability  $\Lambda$  for each source. The underlying values of the EOS parameters are chosen to be consistent with current observational constraints, and we use  $B_{\text{eff}}^{1/4} = 140 \text{ MeV}$ ,  $a_4 = 0.8$ ,  $m_s = 100 \text{ MeV}$  and  $\Delta = 50 \text{ MeV}$  [74, 80]. In this work, we use this fixed but typical configuration to compare the behaviors of the 4-d model and the approximated 2-d model in the Bayesian inference of the EOS.

To include the tidal effects in the waveform, we use the IMRPHENOMXAS waveform model [95–97], and manually add the GW phase correction induced by the tidal deformation at the leading order and next-to-leading order in the frequency domain [21–23]. The phase correction reads

$$\Psi_{\text{Tidal}}(f) = -\frac{39}{2}\tilde{\Lambda}x^5 + \left(-\frac{3115}{64}\tilde{\Lambda} + \frac{6595}{364}\sqrt{1-4\eta\delta\tilde{\Lambda}}\right)x^6, \quad (2.6)$$

where  $M = m_1 + m_2$  is the total mass,  $\eta = m_1 m_2 / M^2$  is the symmetric mass ratio, and  $x = (\pi G M f / c^3)^{2/3}$  is the standard post-Newtonian order parameter. We cut off this correction at the GW frequency corresponding to the Schwarzschild innermost stable circular orbit [98]. Note that both the mass and the frequency are simultaneously taking values in the source frame, or simultaneously in the detector frame, while eq. (2.5) describes mass distribution in the source frame. In the above equation,  $\tilde{\Lambda}$  and  $\delta\tilde{\Lambda}$  are linear combinations of the dimensionless tidal deformabilities of the two stars in the binary system,  $\Lambda_1$  and  $\Lambda_2$ ,

$$\begin{aligned} \tilde{\Lambda} &= \frac{8}{13} \left[ (1 + 7\eta - 31\eta^2)(\Lambda_1 + \Lambda_2) + \sqrt{1 - 4\eta}(1 + 9\eta - 11\eta^2)(\Lambda_1 - \Lambda_2) \right], \\ \delta\tilde{\Lambda} &= \frac{1}{2} \left[ \sqrt{1 - 4\eta} \left( 1 - \frac{13272}{1319}\eta + \frac{8944}{1319}\eta^2 \right) (\Lambda_1 + \Lambda_2) \right. \\ &\quad \left. + \left( 1 - \frac{15910}{1319}\eta + \frac{32850}{1319}\eta^2 + \frac{3380}{1319}\eta^3 \right) (\Lambda_1 - \Lambda_2) \right]. \end{aligned} \quad (2.7)$$

The waveform model is then given by

$$\tilde{h}_{+/\times}(f) = \tilde{h}_{+/\times}^{\text{noTidal}}(f) \cdot e^{-i\Psi_{\text{Tidal}}(f)}, \quad (2.8)$$

where  $\tilde{h}_{+/\times}$  is the plus/cross polarization of the GW signal in the frequency domain, and  $\tilde{h}_{+/\times}^{\text{noTidal}}$  is given by the IMRPHENOMXAS waveform template. As a short summary, the waveform model has 10 parameters, including the binary masses  $m_1$  and  $m_2$ , the luminosity distance  $d_L$ , the merger time  $t_c$ , the right ascension  $\alpha$  and declination  $\delta$ , the inclination angle  $\iota$ , the polarization angle  $\psi$ , and the two tidal deformabilities  $\Lambda_1$  and  $\Lambda_2$ .

For the GW detectors, we choose a ground-based network consisting of two CE detectors and one ET detector, whose sensitivity curves are taken as CE-2 [52–54] and ET-D [50, 51], respectively. The two CE detectors are positioned at the current locations of the two LIGO detectors, while the ET detector is situated at the present Virgo detector site.

### 3 Hierarchical Inference of EOS Parameters

#### 3.1 Principles

The EOS of Qs cannot be directly measured from GW signals. Instead, different EOSs determine different relationship between the tidal deformability and the mass of the compact stars, leading to an impact on the GW signals. In turn, one firstly estimates the masses and the tidal deformabilities of the merging binaries from GW signals, then use them to fit the  $m$ - $\Lambda$  relation and estimate the EOS parameters.

It is expected that the measurement of EOSs requires an appropriate combination of multiple GW events. However, if one naively combines all data and estimate the GW parameters and EOS parameters together, say, in one giant Bayesian PE, the inference would be computationally impractical for a high-dimensional parameter space. To address this issue, we adopt the so-called hierarchical Bayesian inference method, which has been widely used for studying the population properties of compact binaries [59–64, 94]. As its name suggests, the hierarchical inference allows one to conduct inference calculation layer by layer, and estimate the GW parameters (controlling the GW signals) and population hyper-parameters (controlling the prior distribution of the GW parameters) separately. In this study, the EOS parameters can also be regarded as hyper-parameters, which give a deterministic relationship—a  $\delta$ -function-type prior—between  $\Lambda$  and  $m$ . These hyper-parameters can be estimated in the hierarchical Bayesian inference framework [46, 65, 67, 69]. Below we briefly introduce the methodology of the hierarchical inference, and the procedure to apply this technology to infer EOS parameters.

We start from the Bayes’ theorem,

$$P(\mathbf{H}|D) \propto P(D|\mathbf{H})\pi(\mathbf{H}), \quad (3.1)$$

where  $D \equiv \{d_1, d_2, \dots, d_n\}$  denotes all the collected GW data,  $\mathbf{H}$  is the set of hyper-parameters. Specifically, we have  $\mathbf{H} = \{B_{\text{eff}}^{1/4}, a_4, m_s, \Delta\}$  for the 4-d model and  $\mathbf{H} = \{B_{\text{eff}}^{1/4}, \beta\}$  for the 2-d model.  $P(\mathbf{H}|D)$  is the posterior distribution of the hyper-parameters,  $P(D|\mathbf{H})$  is the likelihood function, and  $\pi(\mathbf{H})$  is the prior distribution of the hyper-parameters. As it is the  $i$ -th set of GW parameters  $\theta_i$  that influence the corresponding GW data  $d_i$ , the likelihood  $P(D|\mathbf{H})$  can be written as

$$\begin{aligned} P(D|\mathbf{H}) &= \prod_{i=1}^n \int P(\theta_i|\mathbf{H})P(d_i|\theta_i, \mathbf{H})d\theta_i \\ &= \prod_{i=1}^n \int P(\mathbf{m}_i|\mathbf{H})P(\Lambda_i|\mathbf{m}_i, \mathbf{H})P(\xi_i|\mathbf{m}_i, \Lambda_i, \mathbf{H})P(d_i|\theta_i)d\mathbf{m}_i d\Lambda_i d\xi_i \\ &= \prod_{i=1}^n \int P(\mathbf{m}_i|\mathbf{H})\delta(\Lambda_i - \lambda(\mathbf{m}_i, \mathbf{H}))d\mathbf{m}_i d\Lambda_i \int P(\xi_i)P(d_i|\theta_i)d\xi_i. \end{aligned} \quad (3.2)$$

The first line uses the total probability theorem, under the assumption that different GW events are independent. In the second line, we divide the GW parameters into three categories: the mass parameters  $\mathbf{m}_i$ , the tidal parameters  $\Lambda_i$ , and the nuisance parameters  $\xi_i$ . Note that one can choose different but equivalent representations for mass parameters, namely  $\{m_{1,i}, m_{2,i}\}$  versus  $\{\mathcal{M}_i, \eta_i\}$ , and tidal parameters, namely  $\{\Lambda_{1,i}, \Lambda_{2,i}\}$  versus  $\{\tilde{\Lambda}_i, \delta\tilde{\Lambda}_i\}$ . In the third line, the  $\delta$ -function means that  $\Lambda_i$  is determined by  $\mathbf{m}_i$  and  $\mathbf{H}$  through the EOS

model  $\lambda(\mathbf{m}_i, \mathbf{H})$ , which is given in section 2.1. Besides, we assume that the distributions of nuisance parameters  $\xi_i$  are independent of  $\mathbf{m}_i$ ,  $\Lambda_i$  and  $\mathbf{H}$ .

In the hierarchical inference, the integral of the nuisance parameters,  $\int P(\xi_i)P(d_i|\theta_i)d\xi_i$ , is independent of the hyper-parameters  $\mathbf{H}$ , thus can be calculated in advance to reduce the computational cost [63, 65, 69]. Considering the single-event PE for the  $i$ -th GW event, the posterior of parameters  $\theta_i$  can be written as

$$P(\theta_i|d_i) \propto \pi_{\emptyset}(\theta_i)P(d_i|\theta_i), \quad (3.3)$$

where  $P(d_i|\theta_i)$  is the single-event likelihood [99],

$$L_i(\theta_i) \equiv P(d_i|\theta_i) \propto e^{-\frac{1}{2}(d_i-h(\theta_i), d_i-h(\theta_i))}, \quad (3.4)$$

with  $h(\theta_i)$  given by the waveform model in section 2.2. In eq. (3.4) the inner product  $(u, v)$  is defined as

$$(u, v) := 2\Re \int_{-\infty}^{\infty} \frac{u^*(f)v(f)}{S_n(|f|)} df, \quad (3.5)$$

where  $S_n$  is the power spectral density of the noise of the detector network,  $u(f)$  and  $v(f)$  are the Fourier transforms of  $u(t)$  and  $v(t)$ , respectively. A more detailed description about the single-event likelihood, such as the projection of GWs and combination of different detectors, can be found in ref. [65]. Now we focus on the  $\pi_{\emptyset}(\theta_i)$  in eq. (3.3), which is some *default* prior of  $\theta_i$  chosen for a complete expression of the Bayes' theorem. However, if one chooses  $\pi_{\emptyset}(\theta_i) \propto P(\xi_i)$ , namely, flat priors for mass and tidal parameters and the same marginal distributions in eq. (3.2) for nuisance parameters, the joint posterior distribution of  $\mathbf{m}_i$  and  $\Lambda_i$  will become

$$P(\mathbf{m}_i, \Lambda_i|d_i) = \int P(\theta_i|d_i)d\xi_i \propto \int P(\xi_i)P(d_i|\theta_i)d\xi_i, \quad (3.6)$$

which is just the integral over  $P(\xi_i)$  in eq. (3.2), modulus a constant multiplicative factor.

From above derivation, one finds that eq. (3.3) represents an auxiliary PE, whose posterior can help to calculate the integral on the nuisance parameters in eq. (3.2). In the language of Bayesian analysis, this integral is called the marginal likelihood [100], or the quasi-likelihood [65], which is denoted as  $L_i^q$ ,

$$L_i^q(\mathbf{m}_i, \Lambda_i) = \int P(\xi_i)L_i(\mathbf{m}_i, \Lambda_i, \xi_i)d\xi_i \propto P(\mathbf{m}_i, \Lambda_i|d_i). \quad (3.7)$$

Furthermore, the calculation of posterior in eq.(3.3) is a standard single-event PE, and independent of the hyper-parameters  $\mathbf{H}$ . Thus, one can firstly conduct these auxiliary PEs for each GW event by some sampling techniques, such as the Markov-Chain Monte Carlo (MCMC) method [101–103] and nested sampling [104, 105], and generate samples of the posterior distribution  $P(\theta_i|d_i)$ . Then, the quasi-likelihood  $L_i^q(\mathbf{m}_i, \Lambda_i)$  can be obtained by some density-estimate methods, such as the kernel density estimates, Gaussian processes, and Gaussian mixture models [65, 67, 69, 106–109]. Finally, substituting  $L_i^q$  into eq. (3.2) and completing the integral involving the  $\delta$ -function, the posterior for hyper-parameters becomes,

$$P(\mathbf{H}|D) \propto \pi(\mathbf{H}) \prod_{i=1}^n \int P(\mathbf{m}_i|\mathbf{H})L_i^q(\mathbf{m}_i, \lambda(\mathbf{m}_i, \mathbf{H}))d\mathbf{m}_i, \quad (3.8)$$

which avoids dealing with nuisance parameters and hyper-parameters simultaneously, and makes the computation cost much reduced.



Model	Parameter	True Value	Prior	Posterior
4-d	$B_{\text{eff}}^{1/4}$ (MeV)	140	$\mathcal{U}(130, 150)$	$139.0^{+1.7}_{-1.4}$
	$a_4$	0.8	$\mathcal{U}(0.4, 1.0)$	$0.7^{+0.2}_{-0.2}$
	$m_s$ (MeV)	100	$\mathcal{U}(75, 125)$	$96.8^{+18.1}_{-15.1}$
	$\Delta$ (MeV)	50	$\mathcal{U}(0, 100)$	$41.2^{+14.4}_{-19.6}$
2-d	$B_{\text{eff}}^{1/4}$ (MeV)	140	Flat	$138.2^{+1.5}_{-1.6}$
		140	Transformed	$137.8^{+1.6}_{-1.3}$
	$\beta$ (MeV <sup>2</sup> )	0	Flat	$-1635^{+2297}_{-2229}$
		0	Transformed	$-2415^{+2312}_{-1751}$

**Table 1.** The injected true values and priors of the EOS parameters in 4-d and 2-d models for the Bayesian inference. The corresponding medians and central 68% credible intervals of the posteriors are listed in the last column. Note that the data used in all inferences are generated with the 4-d model.

### 3.2 Implementation

When conducting the single-event PE, we choose  $\mathcal{M}$  and  $\eta$  as the mass parameters, and  $\tilde{\Lambda}$  and  $\delta\tilde{\Lambda}$  as the tidal parameters. Namely, all the parameters we want to recover for a single GW event are  $\boldsymbol{\theta} = \{\mathcal{M}, \eta, \tilde{\Lambda}, \delta\tilde{\Lambda}, d_L, t_c, \alpha, \delta, \psi, \iota\}$ . The priors of  $\mathcal{M}$ ,  $\eta$ ,  $\tilde{\Lambda}$ ,  $\delta\tilde{\Lambda}$  and  $t_c$  are uniform. The prior of  $d_L$  is uniform in comoving volume and source frame time. We adopt the isotropic distribution for the priors of  $\alpha$ ,  $\delta$ ,  $\psi$  and  $\iota$ . Following Lackey and Wade [65], we use the Gaussian kernel density estimator to calculate the quasi-likelihood. We also treat  $\delta\tilde{\Lambda}$  as a nuisance parameter, since it contributes to the waveform at a higher order than  $\tilde{\Lambda}$  [21–23], and therefore it is much less informative for the EOS parameters [65]. Both choices are studied in our work.

For the EOS parameters, we choose flat priors for  $\{B_{\text{eff}}^{1/4}, a_4, m_s, \Delta\}$  around the injected values. While for  $\{B_{\text{eff}}^{1/4}, \beta\}$  in the 2-d model, the prior of  $\beta$  has two choices: (i) it can be chosen to be flat in the allowed range; (ii) it can be generated by the priors of the 4-d model according to the probability density transformation. The latter choice is to ensure a consistent comparison between the 2-d and 4-d models, while the former choice suits for testing the unbiasedness of the 2-d model and avoiding priors’ influence. We summarize the priors of the EOS parameters in table 1.

In PEs of both the single-event parameters and the hyper-parameters, we generate the posterior samples using the BILBY implementation [110] of NESSAI [111–113]. To investigate the 4-d model performance in the EOS inference, we conduct two PEs with the loudest 25 GW events generated in section 2.2. The first PE uses the flat priors in table 1 and focuses on the EOS’s dependence on different parameters. The second one includes some observational constraints for QSSs, giving a more comprehensive forecast for measuring the EOS parameters with the XG GW detectors.

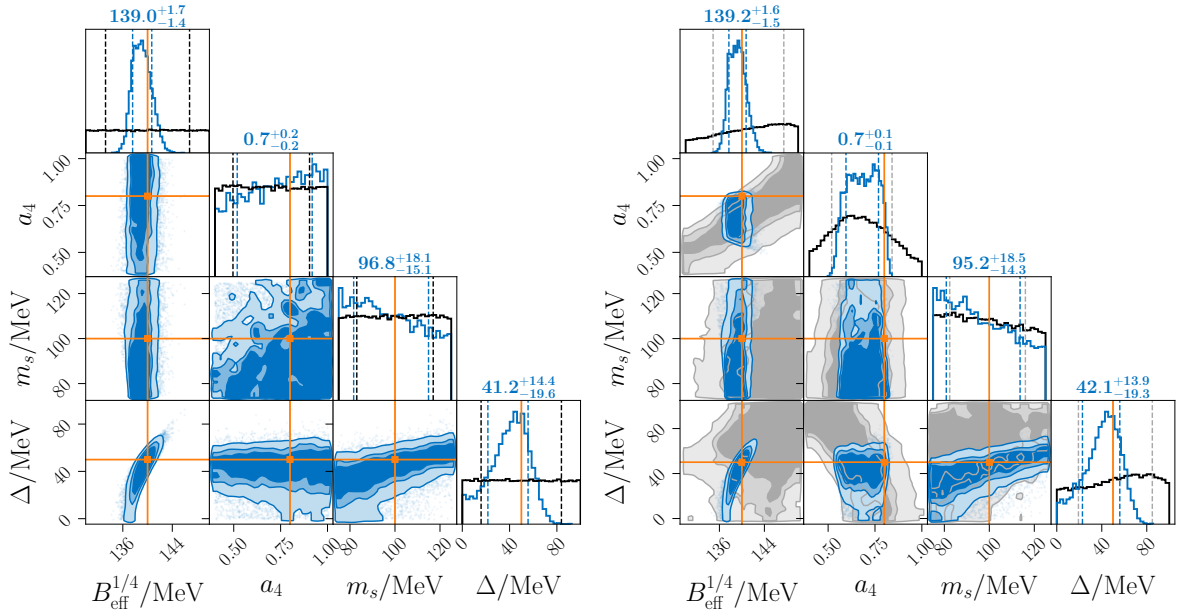


**Figure 2.** Posterior distributions of the EOS parameters in the 4-d model. The contours show 50%, 68% and 90% credible regions. The numbers on the histogram represent the median and the central 68% credible interval of each marginalized distribution. The orange solid line indicates the injected value of EOS parameters. The left panel is for flat priors of EOS parameters, while the right panel further requires stability conditions (see text), which are given by the grey areas, and the constraint from PSR J0740+6620 [91, 114].

## 4 Results and Discussions

### 4.1 Inference of Parameters in the 4-d Model

We summarize the inference results in figure 2 for the 4-d model. In the left panel of figure 2, we show the posterior distribution corresponding to the flat priors. We also show the marginalized posterior distributions, together with their median and the central 68% credible intervals of each parameter in the diagonal. The injected values of the EOS parameters are recovered well, falling into the 68% credible intervals. For  $B_{\text{eff}}^{1/4}$  and  $\Delta$ , the median seems to slightly deviate from the injected value. However, note that the mode of the posterior distribution is just the maximum likelihood estimation (MLE) of the parameters when flat priors are chosen, and the MLE is not necessarily coincident with the median of each parameter. We check that the posterior mode agrees well with the injected values, which can also be observed intuitively by the joint distribution of  $B_{\text{eff}}^{1/4}$  and  $\Delta$  in the lower left corner. The parameters  $a_4$  and  $m_s$  are not well constrained, whose posterior distributions are broad and flat, resembling the priors plotted with black lines. Therefore, the median is also dominated by the priors, which was also observed in refs. [17, 80]. This result is consistent with the fact that  $a_4$  and  $m_s$  only have a weak impact on the  $m$ - $\Lambda$  relation [6, 17, 74, 80]. Besides, We find that  $m_s$  has a slight degeneracy with  $\Delta$ . This originates from the EOS's dependence on the quadratic coefficient  $a_2 = m_s^2 - 4\Delta^2$  [6], which is also the numerator of  $\beta$  in the 2-d model.

When calculating the posterior in the right panel, we further add the stability requirements for Qs in the EOS model: (i) the normal atomic nuclei are more stable than non-strange quark matter; (ii) the SQM is expected to be more stable than normal nuclear

matter [2, 3]. These two constraints are called the “2 flavor” line and the “3 flavor” line respectively [15], and single out a subset in the priors’ parameter space. We plot this constrained region in the corner plot with grey contours, and show the marginalized priors with black lines. Besides, the maximum QS mass of an EOS needs to be large enough to support the known heaviest pulsars. We adopt the mass measurement of PSR J0740+6620 [91, 114],  $m = 2.072^{+0.067}_{-0.066} M_{\odot}$ . With these requirements, the quartic coefficient  $a_4$  is constrained more tightly than in the case of flat priors. This is because that the stability requirements introduce some mild correlations between  $a_4$  and the well-constrained parameters  $B_{\text{eff}}^{1/4}$  and  $\Delta$ .

Thanks to the high sensitivity of XG GW detectors, the measurement precision of  $B_{\text{eff}}^{1/4}$  and  $\Delta$  can be improved by several times compared to the constraints from GW170817 and GW190425 in current-generation detector network [74, 80]. For example, the color-flavor locked pairing gap  $\Delta$  is barely measurable with the current GW detectors, and the reported constraints highly depend on the choices of priors [80]. As a comparison, one can find a significant peak in the marginalized posterior distribution of  $\Delta$  in figure 2. These constraints will be further tightened if more lower-SNR (besides the top 25) events are added into the analysis.

## 4.2 Comparison between 2-d and 4-d Models

In the 4-d model, we find that  $a_4$  and  $m_s$  are not constrained well, and there exists a weak correlation between  $m_s$  and  $\Delta$ . This implies possible redundance in the parameterization of the EOS model. As mentioned in section 2.1, Zhang and Mann [77] proposed a QS model with only 2 parameters,  $B_{\text{eff}}^{1/4}$  and  $\beta$ , reducing the number of degrees of freedom. However, the simplification is based on omitting the fourth and higher-order terms of  $m_s$  in the chemical potential, which may lead to biases in the inference of EOS parameters. In this subsection, we analyze the EOS inferences using the 2-d model and test whether the EOS parameters are recovered correctly.

Like the 4-d model, we show the posterior distributions of  $B_{\text{eff}}^{1/4}$  and  $\beta$  in figure 3. In the left panel, the red and green contours respectively represent the inference results using the flat and transformed priors in table 1. One immediately finds that the injected values are not in the 90% credible region of the posterior distribution. For the marginal distributions, the injected value of  $B_{\text{eff}}^{1/4}$  is also beyond the 68% credible interval, while the injected value of  $\beta$  is close to the upper bound of the 68% credible interval. As a comparison, the 4-d posterior samples in section 4.1 are transformed into the 2-d parameter space and they are plotted in blue. We find that the injected values still fall into the contours in this transformed space. Therefore, we conclude that using the 2-d simplified QS model may introduce systematic biases in the EOS inference with the 25 loudest GW events in the XG GW detectors. It should be emphasized that obvious biases are arising because of the accumulation of high-precision GW events. In the right panel of figure 3, we show the inference results using 2-d and 4-d models with only the 4 loudest GW events. In this case, the statistical uncertainties of the EOS parameters are large enough to hide the biases.

We plot the  $m$ - $\Lambda$  relation in figure 4 according to the posterior samples of the 2-d and 4-d models. We choose the posterior samples of the 4-d model without additional constraints (i.e., posteriors in the left panel of figure 2), while for the 2-d model, we use the posterior samples with transformed priors to ensure a consistent comparison. Even through the inference of the 2-d model has obvious biases in the EOS parameters, the recovered  $m$ - $\Lambda$  relation is very close to that of the 4-d model. The recovered  $m$ - $\Lambda$  relationships in both cases are consistent with

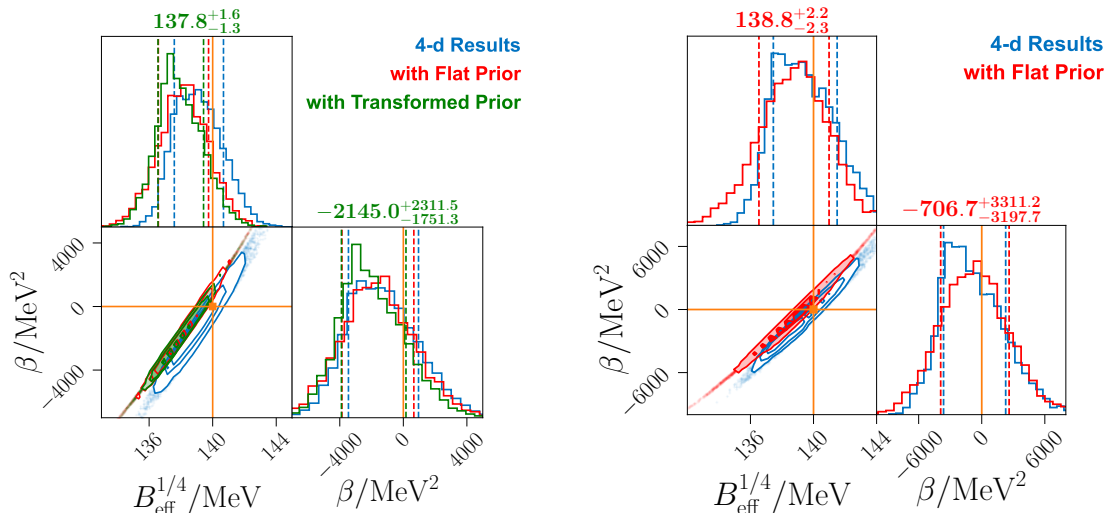


**Figure 3.** Similar to figure 2, but for the 2-d model. The blue contours are drawn according the transformed samples from the 4-d posteriors without observational constraints (i.e., the left panel of figure 2). The red and green contours represent the inference results directly using the 2-d model with two different priors (see table 1). The left panel shows posterior using the 25 loudest GW events in the population, while in the right panel only 4 loudest GW events are used.

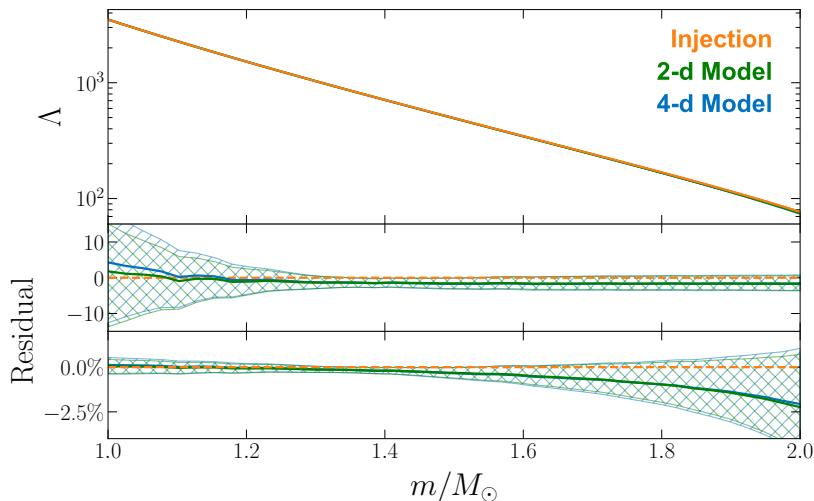


**Figure 4.** The  $m$ - $\Lambda$  relations for the posterior of the 2-d and 4-d EOS models, plotted in green and blue respectively. The orange line represents the injected  $m$ - $\Lambda$  relation. For each QS mass, we show the median and the 68% credible interval of  $\Lambda$ .

the injected EOS within the 68% credible level. This is not surprising, since in this work the EOS parameters are constrained by measuring  $\Lambda$  and  $m$  from the GW events. Furthermore, we find a strong degeneracy between  $B_{\text{eff}}^{1/4}$  and  $\beta$  in the inference of the 2-d model. This may imply that there still exists redundant degrees of freedom in the 2-d QS model, but it is more likely due to the fact that only the tidal parameter of the QS is used to constrain the EOS. Similar degeneracy is also observed when transforming the 4-d posterior samples to the 2-d parameter space. We leave a more detailed study of this degeneracy for future work.

## 5 Summary and Outlook

In this work, we simulated GW observations with an XG GW detector network consisting of two CE detectors and one ET detector, and tested the potential of constraining the EOS of Qs with these GW events. Adopting the hierarchical Bayesian inference method [61, 62, 65], we compared the inference results of the full 4-d model [6] and the simplified 2-d model [77].

From the inference of the 4-d model in figure 2, we found that the constraints on the effective bag constant  $B_{\text{eff}}^{1/4}$  and the pairing energy gap of the color superconductivity  $\Delta$  can be improved by several times with the help of the XG detectors, while the strange quark mass  $m_s$  and the QCD correction parameter  $a_4$  are still poorly constrained. Adding the stability and maximum-mass requirements does not improve the constraints on  $B_{\text{eff}}^{1/4}$  and  $\Delta$ , but slightly tightens the constraint on  $a_4$  because of the mild correlations between  $a_4$  and the well-constrained parameters. Therefore,  $m_s$  and  $a_4$  are not likely to be directly inferred from the tidal deformation measurements of GWs in XG detectors. These results are consistent with the previous studies [6, 17, 74, 80].

Figure 3 showed the inference results of the 2-d and 4-d models, and demonstrated how the PE biases arise with the accumulation of GW events in the 2-d model. When taking the 25 loudest GW events into the analysis, the inference results of the 2-d model show systematic biases in the EOS parameters, while the 4-d model gives unbiased results. If only the top 4 loudest events are used, the statistical uncertainties of the EOS parameters are large enough to cover the biases of the 2-d model. However, the predicted  $m$ - $\Lambda$  relations in both the 2-d and 4-d models are consistent with the injected relation within the 68% credible level, even when 25 loudest GW events are used. Therefore, if one only focuses on the tidal parameter of Qs, the 2-d model is suitable as a simplified and analytical expression of the EOS, providing a smaller parameter space thus faster computation. At the same time, we emphasized that the approximate accuracy of the 2-d model is insufficient to meet the observation precision in the XG GW detections, especially when analyzing large numbers of GW events.

To our knowledge, this study is the first to discuss the hierarchical inference of the QS EOS with a large number of GW events in the XG GW detectors. However, there are still some limitations in this work. First, to obtain an unbiased result for the EOS parameters, the single-event PE should also be unbiased. Some factors, such as the inaccurate waveform model, may lead to non-negligible biases in the measurements of the GW parameters, especially for high-SNR events [115–118]. Besides, considering the high detection rate in the XG detectors, the GW signals may overlap with each other, which can also lead to PE biases [119–121]. Moreover, the spins of the compact stars were ignored in this work. This may lead to an overestimation of the measurement precision of the tidal and mass parameters, thus obtain an optimistic constraint on the EOS parameters. As for the inference at the hyper-parameter level, it is natural to study the inference of the EOS parameters using the whole population. Using GPU acceleration can significantly reduce the computational time of the hierarchical inference including a large number of GW events, and it has been applied to the study of NSs [68]. Some studies also recommended inferring the EOS and the mass distribution simultaneously to avoid possible biases [69, 108]. Finally, we found a tight degeneracy between  $B_{\text{eff}}^{1/4}$  and  $\beta$  in the 2-d QS model. One may combine other information, such as the mass and radius observation or the post-merger remnants to break this degeneracy. The nonradial oscillation of Qs, such as the  $f$  and the  $w_{\text{II}}$  modes, can also leave imprints in GW signals and serve as a probe for EOS inference [45, 49, 122]. We leave these extensions for future work. In conclusion, the XG GW observation has a great potential to constrain the EOS of

compact stars, and future observations will further uncover the properties of dense matter.

## Acknowledgments

This work was supported by the National Natural Science Foundation of China (123B2043, 11991053, 12405065, 12405052), the Beijing Natural Science Foundation (1242018), the National SKA Program of China (2020SKA0120300), the Max Planck Partner Group Program funded by the Max Planck Society, the Fundamental Research Funds for the Central Universities and the High-performance Computing Platform of Peking University.

## References

- [1] N. Itoh, *Prog. Theor. Phys.* **44**, 291 (1970).
- [2] A. R. Bodmer, *Phys. Rev. D* **4**, 1601 (1971).
- [3] E. Witten, *Phys. Rev. D* **30**, 272 (1984).
- [4] C. Alcock, E. Farhi, and A. Olinto, *Astrophys. J.* **310**, 261 (1986).
- [5] P. Haensel, J. L. Zdunik, and R. Schaeffer, *Astron. Astrophys.* **160**, 121 (1986).
- [6] M. Alford, M. Braby, M. W. Paris, and S. Reddy, *Astrophys. J.* **629**, 969 (2005), [arXiv:nucl-th/0411016](#) .
- [7] S. B. Ruester and D. H. Rischke, *Phys. Rev. D* **69**, 045011 (2004), [arXiv:nucl-th/0309022](#) .
- [8] J. E. Horvath and G. Lugones, *Astron. Astrophys.* **422**, L1 (2004), [arXiv:astro-ph/0402349](#) .
- [9] M. Alford, D. Blaschke, A. Drago, T. Klahn, G. Pagliara, and J. Schaffner-Bielich, *Nature* **445**, E7 (2007), [arXiv:astro-ph/0606524](#) .
- [10] T. Fischer, I. Sagert, G. Pagliara, M. Hempel, J. Schaffner-Bielich, T. Rauscher, F. K. Thielemann, R. Kappeli, G. Martinez-Pinedo, and M. Liebendorfer, *Astrophys. J. Suppl.* **194**, 39 (2011), [arXiv:1011.3409 \[astro-ph.HE\]](#) .
- [11] A. Kurkela, P. Romatschke, and A. Vuorinen, *Phys. Rev. D* **81**, 105021 (2010), [arXiv:0912.1856 \[hep-ph\]](#) .
- [12] A. Kurkela, P. Romatschke, A. Vuorinen, and B. Wu, (2010), [arXiv:1006.4062 \[astro-ph.HE\]](#) .
- [13] F. Ozel, D. Psaltis, S. Ransom, P. Demorest, and M. Alford, *Astrophys. J. Lett.* **724**, L199 (2010), [arXiv:1010.5790 \[astro-ph.HE\]](#) .
- [14] J. M. Lattimer and M. Prakash, “What a Two Solar Mass Neutron Star Really Means,” in *From Nuclei to Stars: Festschrift in Honor of Gerald E Brown*, edited by S. Lee (2011) pp. 275–304, [arXiv:1012.3208 \[astro-ph.SR\]](#) .
- [15] S. Weissenborn, I. Sagert, G. Pagliara, M. Hempel, and J. Schaffner-Bielich, *Astrophys. J. Lett.* **740**, L14 (2011), [arXiv:1102.2869 \[astro-ph.HE\]](#) .
- [16] S. Bhattacharyya, I. Bombaci, D. Logoteta, and A. V. Thampan, *Mon. Not. Roy. Astron. Soc.* **457**, 3101 (2016), [arXiv:1601.06120 \[astro-ph.HE\]](#) .
- [17] A. Li, Z.-Q. Miao, J.-L. Jiang, S.-P. Tang, and R.-X. Xu, *Mon. Not. Roy. Astron. Soc.* **506**, 5916 (2021), [arXiv:2009.12571 \[astro-ph.HE\]](#) .
- [18] Y. Gao, X.-Y. Lai, L. Shao, and R.-X. Xu, *Mon. Not. Roy. Astron. Soc.* **509**, 2758 (2021), [arXiv:2109.13234 \[gr-qc\]](#) .
- [19] F. M. da Silva, A. Issifu, L. L. Lopes, L. C. N. Santos, and D. P. Menezes, *Phys. Rev. D* **109**, 043054 (2024), [arXiv:2309.16865 \[nucl-th\]](#) .

- [20] B. P. Abbott *et al.* (LIGO Scientific, Virgo), *Phys. Rev. Lett.* **116**, 061102 (2016), [arXiv:1602.03837 \[gr-qc\]](#) .
- [21] J. Vines, E. E. Flanagan, and T. Hinderer, *Phys. Rev. D* **83**, 084051 (2011), [arXiv:1101.1673 \[gr-qc\]](#) .
- [22] M. Favata, *Phys. Rev. Lett.* **112**, 101101 (2014), [arXiv:1310.8288 \[gr-qc\]](#) .
- [23] L. Wade, J. D. E. Creighton, E. Ochsner, B. D. Lackey, B. F. Farr, T. B. Littenberg, and V. Raymond, *Phys. Rev. D* **89**, 103012 (2014), [arXiv:1402.5156 \[gr-qc\]](#) .
- [24] L. Baiotti, *Prog. Part. Nucl. Phys.* **109**, 103714 (2019), [arXiv:1907.08534 \[astro-ph.HE\]](#) .
- [25] K. Chatziioannou, *Gen. Rel. Grav.* **52**, 109 (2020), [arXiv:2006.03168 \[gr-qc\]](#) .
- [26] E. Annala, C. Ecker, C. Hoyos, N. Jokela, D. Rodríguez Fernández, and A. Vuorinen, *JHEP* **12**, 078 (2018), [arXiv:1711.06244 \[astro-ph.HE\]](#) .
- [27] R. Nandi and P. Char, *Astrophys. J.* **857**, 12 (2018), [arXiv:1712.08094 \[astro-ph.HE\]](#) .
- [28] V. Paschalidis, K. Yagi, D. Alvarez-Castillo, D. B. Blaschke, and A. Sedrakian, *Phys. Rev. D* **97**, 084038 (2018), [arXiv:1712.00451 \[astro-ph.HE\]](#) .
- [29] C.-M. Li, Y. Yan, J.-J. Geng, Y.-F. Huang, and H.-S. Zong, *Phys. Rev. D* **98**, 083013 (2018), [arXiv:1808.02601 \[nucl-th\]](#) .
- [30] R. O. Gomes, P. Char, and S. Schramm, *Astrophys. J.* **877**, 139 (2019), [arXiv:1806.04763 \[nucl-th\]](#) .
- [31] X. Lai, E. Zhou, and R. Xu, *Eur. Phys. J. A* **55**, 60 (2019), [arXiv:1811.00193 \[astro-ph.HE\]](#) .
- [32] B. P. Abbott *et al.* (LIGO Scientific, Virgo), *Phys. Rev. Lett.* **121**, 161101 (2018), [arXiv:1805.11581 \[gr-qc\]](#) .
- [33] N.-B. Zhang and B.-A. Li, *Eur. Phys. J. A* **55**, 39 (2019), [arXiv:1807.07698 \[nucl-th\]](#) .
- [34] Z.-Y. Zhu, E.-P. Zhou, and A. Li, *Astrophys. J.* **862**, 98 (2018), [arXiv:1802.05510 \[nucl-th\]](#) .
- [35] M. F. Carney, L. E. Wade, and B. S. Irwin, *Phys. Rev. D* **98**, 063004 (2018), [arXiv:1805.11217 \[gr-qc\]](#) .
- [36] C. Y. Tsang, M. B. Tsang, P. Danielewicz, W. G. Lynch, and F. J. Fattoyev, *Phys. Lett. B* **796**, 1 (2019), [arXiv:1905.02601 \[nucl-th\]](#) .
- [37] Y. Lim and J. W. Holt, *Eur. Phys. J. A* **55**, 209 (2019), [arXiv:1902.05502 \[nucl-th\]](#) .
- [38] A. Guerra Chaves and T. Hinderer, *J. Phys. G* **46**, 123002 (2019), [arXiv:1912.01461 \[nucl-th\]](#) .
- [39] L. Shao and K. Yagi, *Sci. Bull.* **67**, 1946 (2022), [arXiv:2209.03351 \[gr-qc\]](#) .
- [40] J. L. Ripley, A. Hegade K. R., R. S. Chandramouli, and N. Yunes, (2023), [10.1038/s41550-024-02323-7](#), [arXiv:2312.11659 \[gr-qc\]](#) .
- [41] M. Shibata, S. Fujibayashi, K. Hotokezaka, K. Kiuchi, K. Kyutoku, Y. Sekiguchi, and M. Tanaka, *Phys. Rev. D* **96**, 123012 (2017), [arXiv:1710.07579 \[astro-ph.HE\]](#) .
- [42] A. Bauswein, O. Just, H.-T. Janka, and N. Stergioulas, *Astrophys. J. Lett.* **850**, L34 (2017), [arXiv:1710.06843 \[astro-ph.HE\]](#) .
- [43] M. Ruiz, S. L. Shapiro, and A. Tsokaros, *Phys. Rev. D* **97**, 021501 (2018), [arXiv:1711.00473 \[astro-ph.HE\]](#) .
- [44] M. Shibata, E. Zhou, K. Kiuchi, and S. Fujibayashi, *Phys. Rev. D* **100**, 023015 (2019), [arXiv:1905.03656 \[astro-ph.HE\]](#) .
- [45] H.-B. Li, Y. Gao, L. Shao, R.-X. Xu, and R. Xu, *Mon. Not. Roy. Astron. Soc.* **516**, 6172 (2022), [arXiv:2206.09407 \[gr-qc\]](#) .

- [46] A. W. Criswell, J. Miller, N. Woldemariam, T. Soultanis, A. Bauswein, K. Chatziioannou, M. W. Coughlin, G. Jones, and V. Mandic, *Phys. Rev. D* **107**, 043021 (2023), [arXiv:2211.05250 \[astro-ph.HE\]](#) .
- [47] C. Zhang, Y. Luo, H.-B. Li, L. Shao, and R. Xu, *Phys. Rev. D* **109**, 063020 (2024), [arXiv:2306.08234 \[astro-ph.HE\]](#) .
- [48] Y. Zhou, C. Zhang, J. Zhao, K. Kiuchi, S. Fujibayashi, and E. Zhou, (2024), [arXiv:2407.08544 \[astro-ph.HE\]](#) .
- [49] H.-B. Li, Y. Gao, L. Shao, and R.-X. Xu, *Universe* **10**, 157 (2024).
- [50] D. Reitze *et al.*, *Bull. Am. Astron. Soc.* **51**, 035 (2019), [arXiv:1907.04833 \[astro-ph.IM\]](#) .
- [51] D. Reitze *et al.*, *Bull. Am. Astron. Soc.* **51**, 141 (2019), [arXiv:1903.04615 \[astro-ph.IM\]](#) .
- [52] M. Punturo *et al.*, *Class. Quant. Grav.* **27**, 194002 (2010).
- [53] S. Hild *et al.*, *Class. Quant. Grav.* **28**, 094013 (2011), [arXiv:1012.0908 \[gr-qc\]](#) .
- [54] B. Sathyaprakash *et al.*, *Class. Quant. Grav.* **29**, 124013 (2012), [Erratum: *Class. Quant. Grav.* **30**, 079501 (2013)], [arXiv:1206.0331 \[gr-qc\]](#) .
- [55] B. P. Abbott *et al.* (LIGO Scientific, Virgo), *Phys. Rev. Lett.* **120**, 091101 (2018), [arXiv:1710.05837 \[gr-qc\]](#) .
- [56] B. S. Sathyaprakash *et al.*, *Bull. Am. Astron. Soc.* **51**, 251 (2019), [arXiv:1903.09221 \[astro-ph.HE\]](#) .
- [57] V. Kalogera *et al.*, (2021), [arXiv:2111.06990 \[gr-qc\]](#) .
- [58] A. Samajdar, J. Janquart, C. Van Den Broeck, and T. Dietrich, *Phys. Rev. D* **104**, 044003 (2021), [arXiv:2102.07544 \[gr-qc\]](#) .
- [59] I. Mandel, *Phys. Rev. D* **81**, 084029 (2010), [arXiv:0912.5531 \[astro-ph.HE\]](#) .
- [60] I. Mandel and R. O’Shaughnessy, *Class. Quant. Grav.* **27**, 114007 (2010), [arXiv:0912.1074 \[astro-ph.HE\]](#) .
- [61] M. R. Adams, N. J. Cornish, and T. B. Littenberg, *Phys. Rev. D* **86**, 124032 (2012), [arXiv:1209.6286 \[gr-qc\]](#) .
- [62] I. Mandel, W. M. Farr, and J. R. Gair, *Mon. Not. Roy. Astron. Soc.* **486**, 1086 (2019), [arXiv:1809.02063 \[physics.data-an\]](#) .
- [63] E. Thrane and C. Talbot, *Publ. Astron. Soc. Austral.* **36**, e010 (2019), [Erratum: *Publ. Astron. Soc. Austral.* **37**, e036 (2020)], [arXiv:1809.02293 \[astro-ph.IM\]](#) .
- [64] R. Abbott *et al.* (KAGRA, VIRGO, LIGO Scientific), *Phys. Rev. X* **13**, 011048 (2023), [arXiv:2111.03634 \[astro-ph.HE\]](#) .
- [65] B. D. Lackey and L. Wade, *Phys. Rev. D* **91**, 043002 (2015), [arXiv:1410.8866 \[gr-qc\]](#) .
- [66] S. Bose, K. Chakravarti, L. Rezzolla, B. S. Sathyaprakash, and K. Takami, *Phys. Rev. Lett.* **120**, 031102 (2018), [arXiv:1705.10850 \[gr-qc\]](#) .
- [67] P. Landry and R. Essick, *Phys. Rev. D* **99**, 084049 (2019), [arXiv:1811.12529 \[gr-qc\]](#) .
- [68] C. Talbot and E. Thrane, *Astrophys. J.* **927**, 76 (2022), [arXiv:2012.01317 \[gr-qc\]](#) .
- [69] J. Golomb and C. Talbot, *Astrophys. J.* **926**, 79 (2022), [arXiv:2106.15745 \[astro-ph.HE\]](#) .
- [70] P. K. Gupta, A. Puecher, P. T. H. Pang, J. Janquart, G. Koekoek, and C. Broeck Van Den, (2022), [arXiv:2205.01182 \[gr-qc\]](#) .
- [71] F. Iacovelli, M. Mancarella, C. Mondal, A. Puecher, T. Dietrich, F. Gulminelli, M. Maggiore, and M. Oertel, *Phys. Rev. D* **108**, 122006 (2023), [arXiv:2308.12378 \[gr-qc\]](#) .



- [72] B. Biswas, E. Smyrniotis, I. Liodis, and N. Stergioulas, *Phys. Rev. D* **109**, 064048 (2024), [arXiv:2309.05420 \[gr-qc\]](#) .
- [73] K. Walker, R. Smith, E. Thrane, and D. J. Reardon, *Phys. Rev. D* **110**, 043013 (2024), [arXiv:2401.02604 \[astro-ph.HE\]](#) .
- [74] E.-P. Zhou, X. Zhou, and A. Li, *Phys. Rev. D* **97**, 083015 (2018), [arXiv:1711.04312 \[astro-ph.HE\]](#) .
- [75] S.-H. Yang, C.-M. PI, X.-P. Zheng, and F. Weber, *Astrophys. J.* **902**, 32 (2020), [arXiv:1909.00933 \[astro-ph.HE\]](#) .
- [76] I. Bombaci, A. Drago, D. Logoteta, G. Pagliara, and I. Vidaña, *Phys. Rev. Lett.* **126**, 162702 (2021), [arXiv:2010.01509 \[nucl-th\]](#) .
- [77] C. Zhang and R. B. Mann, *Phys. Rev. D* **103**, 063018 (2021), [arXiv:2009.07182 \[astro-ph.HE\]](#) .
- [78] Z. Cao, L.-W. Chen, P.-C. Chu, and Y. Zhou, *Phys. Rev. D* **106**, 083007 (2022), [arXiv:2009.00942 \[astro-ph.HE\]](#) .
- [79] O. Lourenço, C. H. Lenzi, M. Dutra, E. J. Ferrer, V. de la Incera, L. Paulucci, and J. E. Horvath, *Phys. Rev. D* **103**, 103010 (2021), [arXiv:2104.07825 \[astro-ph.HE\]](#) .
- [80] Z. Miao, J.-L. Jiang, A. Li, and L.-W. Chen, *Astrophys. J. Lett.* **917**, L22 (2021), [arXiv:2107.13997 \[astro-ph.HE\]](#) .
- [81] S.-H. Yang, C.-M. Pi, X.-P. Zheng, and F. Weber, *Phys. Rev. D* **103**, 043012 (2021), [arXiv:2101.11192 \[astro-ph.HE\]](#) .
- [82] S.-H. Yang, C.-M. Pi, and X.-P. Zheng, *Phys. Rev. D* **104**, 083016 (2021), [arXiv:2103.05159 \[astro-ph.HE\]](#) .
- [83] J. D. V. Arbañil, C. V. Flores, C. H. Lenzi, and J. M. Z. Pretel, *Phys. Rev. D* **107**, 124016 (2023), [arXiv:2305.13468 \[astro-ph.HE\]](#) .
- [84] P. T. Oikonomou and C. C. Moustakidis, *Phys. Rev. D* **108**, 063010 (2023), [arXiv:2304.12209 \[astro-ph.HE\]](#) .
- [85] S. Podder, S. Pal, D. Sen, and G. Chaudhuri, *Nucl. Phys. A* **1042**, 122796 (2024), [arXiv:2311.08962 \[nucl-th\]](#) .
- [86] E. S. Fraga, R. D. Pisarski, and J. Schaffner-Bielich, *Phys. Rev. D* **63**, 121702 (2001), [arXiv:hep-ph/0101143](#) .
- [87] C. Xia, Z. Zhu, X. Zhou, and A. Li, *Chin. Phys. C* **45**, 055104 (2021), [arXiv:1906.00826 \[nucl-th\]](#) .
- [88] M. G. Alford, K. Rajagopal, S. Reddy, and F. Wilczek, *Phys. Rev. D* **64**, 074017 (2001), [arXiv:hep-ph/0105009](#) .
- [89] T. Hinderer, *Astrophys. J.* **677**, 1216 (2008), [Erratum: *Astrophys. J.* 697, 964 (2009)], [arXiv:0711.2420 \[astro-ph\]](#) .
- [90] E. Farhi and R. L. Jaffe, *Phys. Rev. D* **30**, 2379 (1984).
- [91] T. E. Riley *et al.*, *Astrophys. J. Lett.* **918**, L27 (2021), [arXiv:2105.06980 \[astro-ph.HE\]](#) .
- [92] N. Farrow, X.-J. Zhu, and E. Thrane, *Astrophys. J.* **876**, 18 (2019), [arXiv:1902.03300 \[astro-ph.HE\]](#) .
- [93] N. Aghanim *et al.* (Planck), *Astron. Astrophys.* **641**, A6 (2020), [Erratum: *Astron. Astrophys.* 652, C4 (2021)], [arXiv:1807.06209 \[astro-ph.CO\]](#) .
- [94] B. P. Abbott *et al.* (LIGO Scientific, Virgo), *Astrophys. J. Lett.* **892**, L3 (2020), [arXiv:2001.01761 \[astro-ph.HE\]](#) .

- [95] G. Pratten, S. Husa, C. Garcia-Quiros, M. Colleoni, A. Ramos-Buades, H. Estelles, and R. Jaume, *Phys. Rev. D* **102**, 064001 (2020), [arXiv:2001.11412 \[gr-qc\]](#) .
- [96] C. García-Quirós, M. Colleoni, S. Husa, H. Estellés, G. Pratten, A. Ramos-Buades, M. Mateu-Lucena, and R. Jaume, *Phys. Rev. D* **102**, 064002 (2020), [arXiv:2001.10914 \[gr-qc\]](#) .
- [97] G. Pratten *et al.*, *Phys. Rev. D* **103**, 104056 (2021), [arXiv:2004.06503 \[gr-qc\]](#) .
- [98] M. Favata, *Phys. Rev. D* **83**, 024027 (2011), [arXiv:1008.4622 \[gr-qc\]](#) .
- [99] L. S. Finn, *Phys. Rev. D* **46**, 5236 (1992), [arXiv:gr-qc/9209010](#) .
- [100] T. J. Loredo and R. L. Wolpert, (2024), [arXiv:2406.18905 \[stat.ME\]](#) .
- [101] N. Christensen and R. Meyer, *Phys. Rev. D* **58**, 082001 (1998).
- [102] N. Christensen, R. J. Dupuis, G. Woan, and R. Meyer, *Phys. Rev. D* **70**, 022001 (2004), [arXiv:gr-qc/0402038](#) .
- [103] S. Sharma, *Ann. Rev. Astron. Astrophys.* **55**, 213 (2017), [arXiv:1706.01629 \[astro-ph.IM\]](#) .
- [104] J. Skilling, in *Bayesian Inference and Maximum Entropy Methods in Science and Engineering*, American Institute of Physics Conference Series, Vol. 735 (2004) p. 395.
- [105] J. Skilling, *Bayesian Analysis* **1**, 833 (2006).
- [106] M. Rosenblatt, *The Annals of Mathematical Statistics* **27**, 832 (1956).
- [107] C. Edward, MIT Press **211**, 212 (2006).
- [108] D. Wysocki, R. O’Shaughnessy, L. Wade, and J. Lange, (2020), [arXiv:2001.01747 \[gr-qc\]](#) .
- [109] V. D’Emilio, R. Green, and V. Raymond, *Mon. Not. Roy. Astron. Soc.* **508**, 2090 (2021), [arXiv:2104.05357 \[gr-qc\]](#) .
- [110] G. Ashton *et al.*, *Astrophys. J. Suppl.* **241**, 27 (2019), [arXiv:1811.02042 \[astro-ph.IM\]](#) .
- [111] M. J. Williams, “nessai: Nested sampling with artificial intelligence,” (2021).
- [112] M. J. Williams, J. Veitch, and C. Messenger, *Phys. Rev. D* **103**, 103006 (2021), [arXiv:2102.11056 \[gr-qc\]](#) .
- [113] M. J. Williams, J. Veitch, and C. Messenger, *Mach. Learn. Sci. Tech.* **4**, 035011 (2023), [arXiv:2302.08526 \[astro-ph.IM\]](#) .
- [114] H. T. Cromartie *et al.* (NANOGrav), *Nature Astron.* **4**, 72 (2019), [arXiv:1904.06759 \[astro-ph.HE\]](#) .
- [115] C. Cutler and M. Vallisneri, *Phys. Rev. D* **76**, 104018 (2007), [arXiv:0707.2982 \[gr-qc\]](#) .
- [116] A. R. Williamson, J. Lange, R. O’Shaughnessy, J. A. Clark, P. Kumar, J. Calderón Bustillo, and J. Veitch, *Phys. Rev. D* **96**, 124041 (2017), [arXiv:1709.03095 \[gr-qc\]](#) .
- [117] M. Pürrer and C.-J. Haster, *Phys. Rev. Res.* **2**, 023151 (2020), [arXiv:1912.10055 \[gr-qc\]](#) .
- [118] R. Gamba, M. Breschi, S. Bernuzzi, M. Agathos, and A. Nagar, *Phys. Rev. D* **103**, 124015 (2021), [arXiv:2009.08467 \[gr-qc\]](#) .
- [119] E. Pizzati, S. Sachdev, A. Gupta, and B. Sathyaprakash, *Phys. Rev. D* **105**, 104016 (2022), [arXiv:2102.07692 \[gr-qc\]](#) .
- [120] Q. Hu and J. Veitch, *Astrophys. J.* **945**, 103 (2023), [arXiv:2210.04769 \[gr-qc\]](#) .
- [121] Z. Wang, D. Liang, J. Zhao, C. Liu, and L. Shao, *Class. Quant. Grav.* **41**, 055011 (2024), [arXiv:2304.06734 \[astro-ph.IM\]](#) .
- [122] H. Sotani, K. Kohri, and T. Harada, *Phys. Rev. D* **69**, 084008 (2004), [arXiv:gr-qc/0310079](#) .